Effect of heat treatments on the microstructure and mechanical properties of directionally solidified multiphase intermetallic Ni-Al-Cr-Ta-Mo-Zr alloy

J. Lapin[1]*, J. Mareček[1], M. Kursa[2]

[1] *Institute of Materials and Machine Mechanics, Slovak Academy of Sciences, Račianska 75, 831 02 Bratislava, Slovak Republic*
[2] *Faculty of Metallurgy and Materials Engineering, VŠB-Technical University of Ostrava, 17. listopadu 15, 708 33 Ostrava-Poruba, Czech Republic*

Received 2 January 2006, accepted 17 January 2006

Abstract

The effect of heat treatments on the microstructure and mechanical properties of directionally solidified (DS) multiphase intermetallic Ni-21.9Al-8.1Cr-4.2Ta-0.9Mo-0.3Zr (in at.%) alloy was studied. Two-step solution annealing of DS alloy at 1373 K for 100 h and 1483 K for 2 h leads to dissolution of spherical α-Cr and needle-like $\gamma'(Ni_3Al)$ precipitates within the β(NiAl) dendrites. In the interdendritic region, dissolution of Cr-based particles and formation of irregular shaped γ areas in the vicinity of dendritic-interdendritic interfaces were observed. During ageing at temperatures from 1223 to 1323 K the growth of spherical α-Cr and lath-shaped γ' precipitates in the β dendrites was observed. In the interdendritic region, the ageing leads to intensive precipitation of lath-shaped α-Cr precipitates, formation of irregular shaped Cr-based particles and transformation of γ matrix (Ni-based solid solution) with γ' precipitates to the γ' matrix with needle-like γ precipitates. The studied heat treatments can be successfully applied to soften the DS alloy. All Vickers hardness values measured for specimens aged at 1273 and 1323 K are lower than those for DS samples. A linear relationship between the Vickers hardness and compressive yield strength is determined for DS and heat-treated (HT) specimens, which allows the mechanical properties of the alloy to be predicted from simple hardness measurements. Optimal combination of the yield strength, ultimate compressive strength and plastic deformation to fracture is achieved after ageing at 1323 K for 30 h.

K e y w o r d s: nickel aluminides, Ni_3Al, NiAl, microstructure, heat treatment, mechanical properties

1. Introduction

Intermetallic alloys based on NiAl and Ni_3Al are potential materials for high-temperature structural applications. Although the mechanical properties of Ni-based intermetallics are attractive, current industrial usage is mainly in corrosion-related structural applications [1–3]. Continuous effort to develop cast Ni--based intermetallics with significantly improved mechanical properties when compared to iron aluminides [4–6], which might also compete with emerging class of cast TiAl-based alloys at intermediate temperatures [7–9] and nickel-based single crystalline superalloys at higher temperatures [10–12] resulted in a group of multiphase intermetallic alloys. These materials can provide a good combination of room-temperature tensile ductility, oxidation resistance, strength and creep resistance that cannot be achieved in monolithic intermetallics [13–19]. Among various systems, directionally solidified (DS) Zr-doped intermetallic Ni--Al-Cr-Ta-Mo alloys with $\gamma'(Ni_3Al)/\gamma$(Ni-based solid solution)-β(NiAl) type of microstructure [16] were developed to improve room-temperature ductility and to achieve superior creep strength at intermediate tem-

*Corresponding author: tel.: +421 2 49268290; fax: +421 2 44253301; e-mail address: ummslapi@savba.sk

Table 1. EDS analysis of dendrites and interdendritic region of DS alloy after two-step solution annealing at 1373 K/100 h and 1483 K/2 h followed by gas fan cooling (in at.%)

Region	Ni	Al	Cr	Ta	Mo	Zr
Dendrites (D)	57.1 ± 0.8	35.4 ± 1.1	5.8 ± 0.4	0.5 ± 0.1	0.9 ± 0.2	0.3 ± 0.1
Interdendritic region (I)	66.5 ± 1.1	14.8 ± 1.2	15.2 ± 0.9	2.2 ± 0.3	0.9 ± 0.1	0.4 ± 0.2
Interdendritic region (II)	66.3 ± 1.4	23.3 ± 1.5	3.9 ± 0.4	5.8 ± 0.5	0.7 ± 0.2	not detected

peratures compared to those of similar alloys based on the β-phase [20, 21]. As shown in our previous study on DS Ni-21.7Al-8.1Cr-6.5Ti (in at.%) alloy [22], critical resolved shear stress for possible slip systems in the precipitation and solid solution strengthened dendrites are higher than their cleavage stress. In order to achieve room-temperature ductility and optimize mechanical properties for specific structural applications, the microstructure of such complex alloys should be carefully controlled during post-solidification heat treatments [14, 16, 22, 23].

The aim of this paper is to study the effect of heat treatments on the microstructure and room-temperature mechanical properties of DS intermetallic multiphase Ni-Al-Cr-Ta-Mo-Zr alloy. As shown in our recent work [24], all DS specimens of the studied Ni-Al-Cr-Ta-Mo-Zr alloy showed very limited or no room-temperature ductility due to premature fracture of dendrites during tensile testing. Therefore, in this study, a special attention is paid to microstructure control of the dendrites with the aim to soften these inherently brittle regions and to improve room-temperature ductility of the studied alloy by appropriate selection of heat treatment parameters.

2. Experimental procedure

The master ingots of intermetallic alloy with the chemical composition Ni-21.9Al-8.1Cr-4.2Ta-0.9Mo-0.3Zr (in at.%) were prepared by plasma arc melting and cast into graphite moulds in an induction furnace under argon atmosphere. These ingots were machined to rods with a length of 100 mm and placed into high purity alumina crucibles of 8/12 mm diameter (inside/outside diameter). Directional solidification was performed under an argon atmosphere in a modified Bridgman-type apparatus described elsewhere [25]. Specimens were directionally solidified at a constant growth rate of $V = 5.56 \times 10^{-5}$ m·s^{-1} and a constant temperature gradient at the solid-liquid interface of $G = 12 \times 10^3$ K·m^{-1}.

All DS ingots were subjected to two-step solution annealing at 1373 K for 100 h and at 1483 K for 2 h. After gas fan cooling to room temperature, ageing at three temperatures of 1223, 1273 and 1323 K for various times ranging from 1 to 100 h was applied. After each ageing step the Vickers hardness and microhardness measurements were performed at the loads of 294 and 0.42 N, respectively. The microhardness measurements were performed on polished and slightly etched transverse sections of ingots.

Compression specimens with a diameter of 6 mm and length of 10 mm were machined from the ingots subjected to two-step solution annealing and ageing at temperature of 1323 K. The compression axis of the specimens was parallel to the [001] growth direction of dendrites. Room-temperature compression tests were performed with a computer-controlled universal testing machine at a strain rate of 2.78×10^{-4} s^{-1}. The offset compressive yield stress was measured at 0.2% plastic strain and ultimate compressive strength was determined as a maximum stress from engineering stress-strain curves.

Microstructural analysis was performed by light optical microscopy (OM), scanning electron microscopy (SEM) and energy dispersive X-ray spectroscopy (EDS). OM and SEM samples were prepared using standard metallographic techniques and etched in a reagent of 150 ml H_2O, 25 ml HNO_3 and 10 ml HF. Volume fraction of coexisting phases and size of precipitates were measured by computerized image analyzer.

3. Results

3.1. Microstructure

3.1.1. Microstructure after directional solidification

After directional solidification at a constant growth rate of 5.56×10^{-5} m·s^{-1} the microstructure of the Ni-21.9Al-8.1Cr-4.2Ta-0.9Mo-0.3Zr (in at.%) alloy consisted of several columnar dendritic grains (3–4). The microstructure contains 58.3 vol.% of dendrites and 41.7 vol.% of interdendritic region. The dendrites grow in [001] crystallographic direction parallel to the ingot axis. The typical dendritic microstructure with well-developed secondary and tertiary dendritic arms is illustrated in Fig. 1a. As resulted from a detailed TEM analysis described elsewhere [26], the dendrites are composed of β matrix with B2 crystal structure, needle-like γ' particles with $L1_2$ crystal structure and spherical α-Cr precipitates with A2 crystal structure,

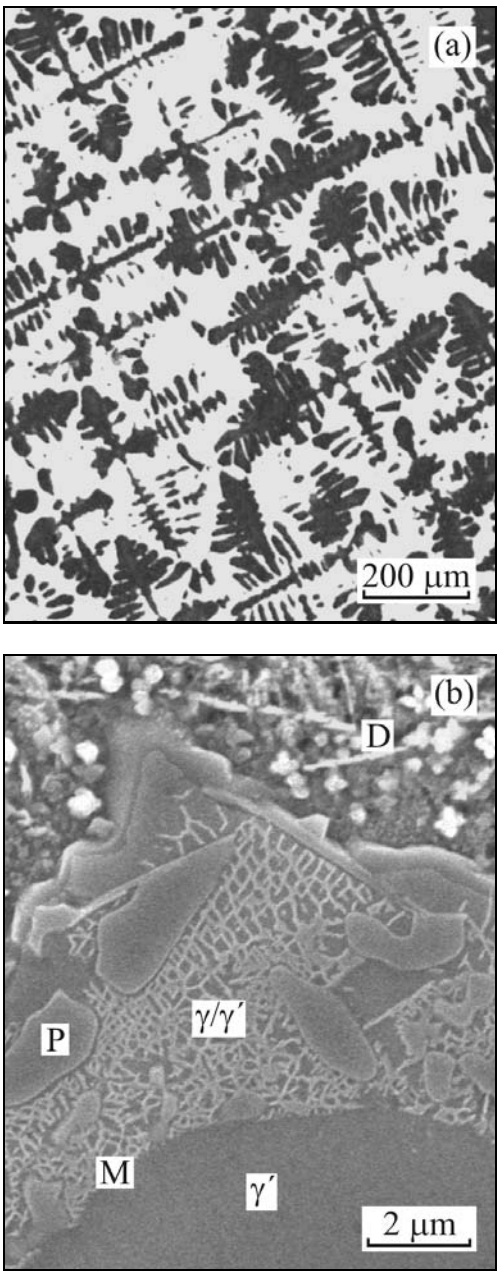

Fig. 1. The typical microstructure of DS alloy: (a) optical micrograph of transverse section showing dendrites with well-developed secondary and tertiary dendrite arms; (b) SEM micrograph showing microstructure of dendrites (D) and interdendritic region (M). P – Cr-based particles.

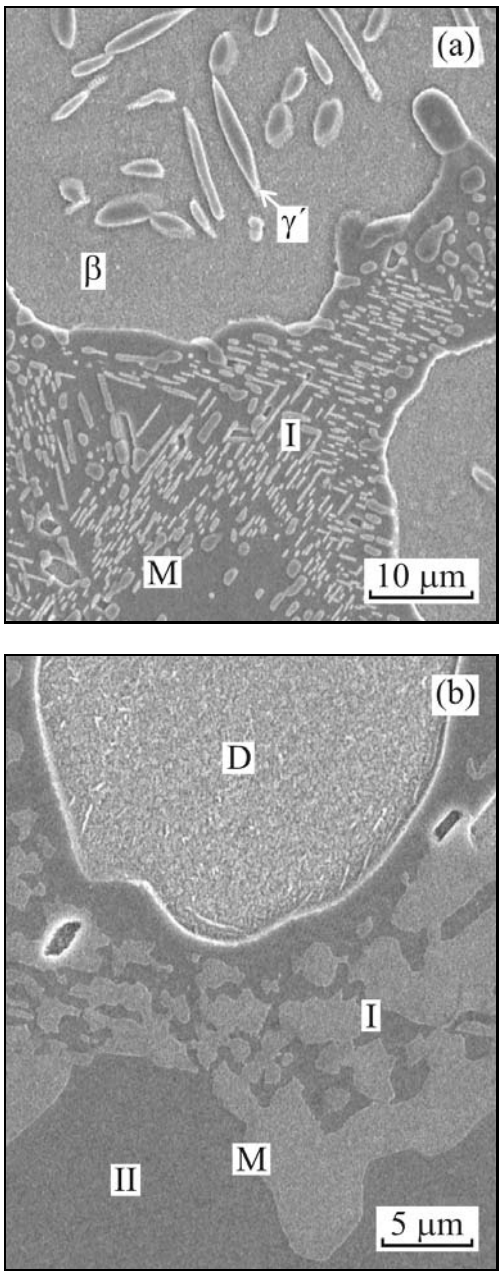

Fig. 2. SEM micrographs showing the microstructure after solution heat treatments: (a) annealing at 1373 K for 100 h and gas fan cooling to room temperature; (b) annealing at 1488 K for 2 h and gas fan cooling to room temperature. D – dendrite, M – interdendritic region (areas I and II).

as illustrated in Fig. 1b. The interdendritic region contains two microstructurally different areas designated as I and II. Interdendritic region I contains three phases: γ matrix with A1 crystal structure, cuboidal and spherical γ' precipitates and irregular Cr-based particles with the chemical composition Cr-32.5Ni--5.9Al-0.5Ta-14Mo-0.7Zr (in at.%). In spite of the previous work on phase composition of the studied alloy [26], the type of the Cr-based particles has not been identified yet. The interdendritic region II contains single γ'-phase.

3.1.2. Effect of solution annealing on microstructure

Figure 2a shows the typical microstructure after the first step of the solution annealing at 1373 K for 100 h. It is clear that a complete dissolution of α--Cr precipitates is achieved after this heat treatment.

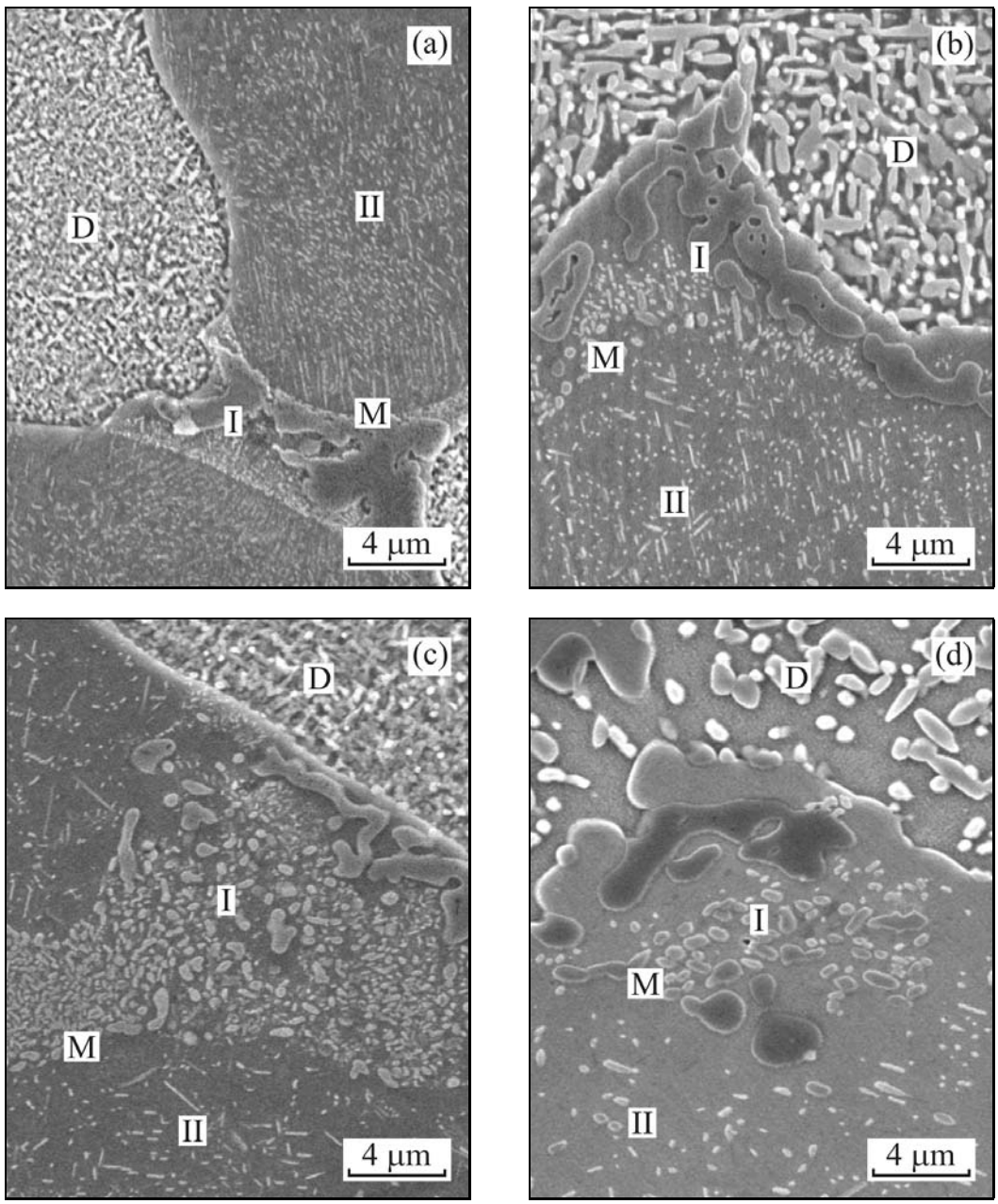

Fig. 3. SEM micrographs showing the effect of ageing on the microstructure: (a) 1223 K/1 h; (b) 1223 K/100 h; (c) 1323 K/1 h; (d) 1323 K/100 h. D – dendrite, M – interdendritic region (areas I and II).

However, coarse elongated γ' particles still remain in the β-phase. The main microstructure change observed in the interdendritic region I is a partial dissolution of Cr-rich particles and transformation of the cuboidal γ/γ' microstructure to the γ' matrix and elongated γ particles. The microstructure in the interdendritic region II remains unchanged and only single γ'-phase is observed. After the second step of the solution annealing at 1483 K for 2 h followed by gas fan cooling to room temperature, a complete dissolution of α-Cr and γ' precipitates within the dendrites is achieved. However, relatively slow cooling rate resulting from gas fan cooling leads to formation of very fine precipitates within the dendrites, as shown in Fig. 2b. This cooling leads to formation of martensitic β'(NiAl) with $L1_0$ crystal structure instead of the β--phase within the dendrites, which is similar to that observed in DS Ni-20.2Al-8.2Cr-2.4Fe or plasma sprayed Ni-30Al (in at.%) alloys described previously by Lapin et al. [29] and Iždinský et al. [30], respectively.

In the interdendritic region I, a complete dissolution of Cr-rich particles is observed and continuous irregular shaped γ-phase areas are formed within the

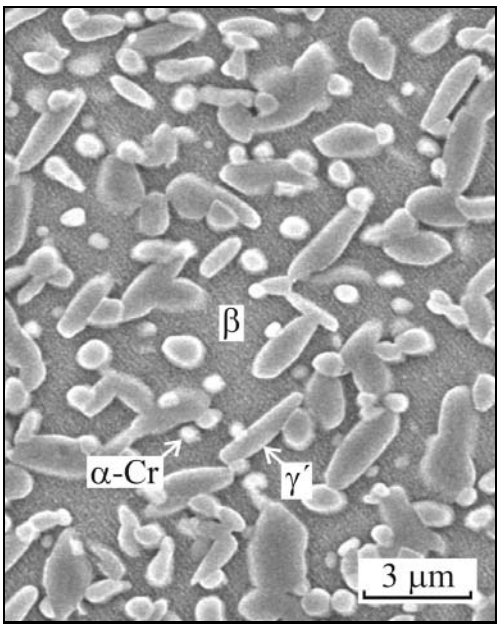

Fig. 4. SEM micrograph showing the typical morphology and distribution of α-Cr and γ' precipitates in the β dendrites after ageing at 1323 K for 100 h.

γ'-phase in the vicinity of the dendrites, as shown in Fig. 2b. Using SEM analysis, no notable microstructural change was observed in the interdendritic region II when compared to that of DS specimens.

3.1.3. Effect of ageing on microstructure

Figure 3 shows the typical microstructures of the specimens after ageing. During early stages of ageing in the temperature range from 1223 to 1323 K the martensitic β'-phase transforms to the β(NiAl). Beside the transformation of the β'-phase, intensive precipitation and growth of spherical α-Cr and needle-like γ' particles within the dendrites are observed. As illustrated in Figs. 3a to 3d, size of the precipitates is significantly affected by the ageing time and temperature. However, the morphology and homogenous distribution of the precipitates within all dendrites arms is preserved, as seen in Fig. 4. Measured statistical data of α-Cr precipitate diameter (minimum 500 precipitates measured at each ageing regime) were fitted by a log-normal distribution function. Figure 5a shows examples of log-normal distribution curves of measured α-Cr precipitate diameter after ageing at 1323 K. The size of α-Cr precipitates increases with increasing ageing time and temperature, as summarized in Fig. 5b. Figure 4 indicates that the needle-like γ' precipitates are nearly round on cross sections. Since aspect ratio A of these precipitates defined as $A = l/d$, where l is the length and d is the diameter of precipitates, was nearly constant during ageing at all temperatures

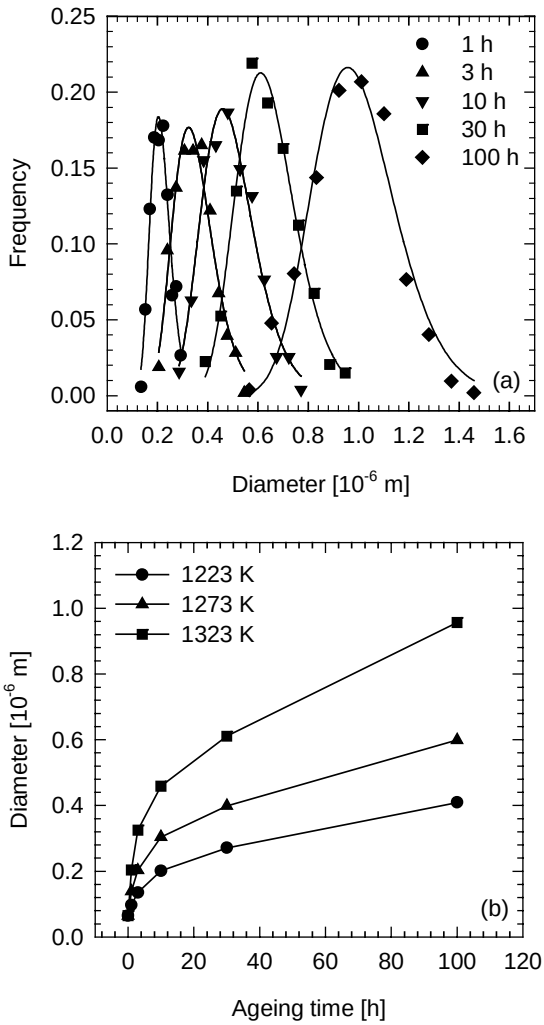

Fig. 5. (a) Example of log-normal distribution curves for diameter of α-Cr precipitates in the β dendrites after ageing at 1323 K. The ageing time is indicated in the figure. (b) Variation of mean α-Cr diameter with the ageing time. The ageing temperatures are indicated in the figure.

and time (about 3), these precipitates are replaced by spherical particles of the equivalent volume. Figure 6a shows examples of log-normal distribution curves of equivalent γ' precipitate diameter after ageing at 1323 K. Mean diameter of the γ' precipitates increases with increasing ageing time and temperature, as summarized in Fig. 6b. Figure 7 illustrates dependence of volume fraction of dendrites on the ageing time. The volume fraction of dendrites decreases with increasing ageing time and temperature. A quasi-equilibrium volume fraction is achieved after ageing at 1323 K for 30 h. On the other hand, the ageing time of 100 h is too short to reach equilibrium volume fractions between the dendrites and interdendritic region for ageing temperatures of 1223 and 1273 K.

During ageing the microstructure within the interdendritic region changed. As seen in Fig. 3, the γ

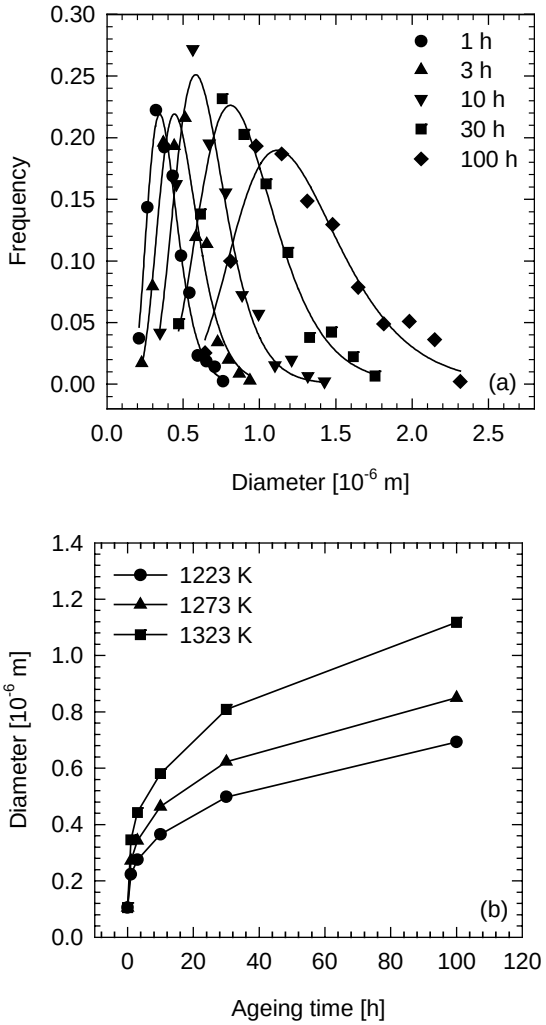

Fig. 6. (a) Example of log-normal distribution curves for equivalent diameter of γ' precipitate in the β dendrites after ageing at 1323 K. The ageing time is indicated in the figure. (b) Variation of mean γ' precipitate diameter with the ageing time. The ageing temperatures are indicated in the figure.

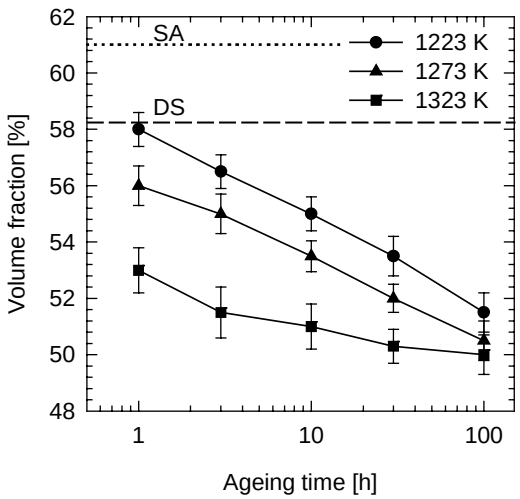

Fig. 7. Dependence of volume fraction of dendrites on the ageing time. The dashed and dotted lines represent volume fractions of dendrites after directional solidification (DS) and solution annealing (SA), respectively. The ageing temperatures are indicated in the figure.

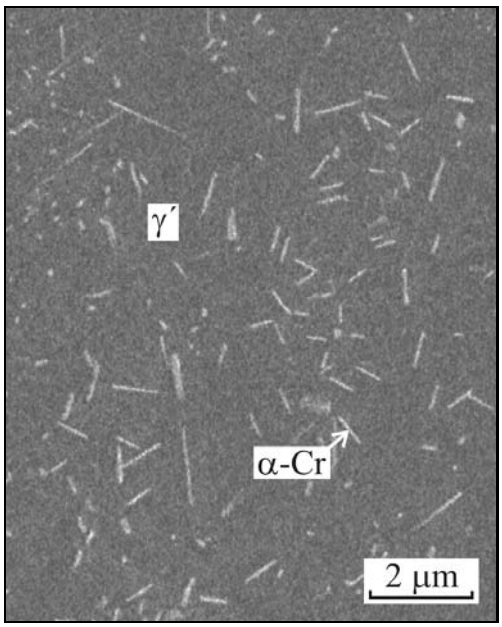

Fig. 8. SEM micrograph showing the typical microstructure of the interdendritic region (area II) after ageing at 1323 K for 1 h.

matrix with γ' precipitates changed to the γ' matrix, elongated γ particles and irregular shaped Cr-rich precipitates in the interdendritic region I. Intensive precipitation of lath-shaped α-Cr particles in the γ' matrix is observed in the interdendritic region II, as shown in Fig. 8.

3.2. Mechanical properties

3.2.1. Effect of heat treatments on Vickers hardness and microhardness

Figure 9 shows variation of Vickers microhardness of dendrites, interdendritic regions I and II with the ageing time. As seen in Fig. 9a, increasing ageing time and temperature lead to a decrease of the microhardness of the dendrites. It is clear that the applied heat treatments lead to a softening of the dendrites when compared to DS specimens (dashed line). A significant microhardness decrease of the aged samples when compared to that of solution annealed (SA) ones (dotted line) can be attributed to the transformation of martensitic β' to the β-phase. A minimum microhardness of 2.77 GPa is achieved after ageing at 1323 K for 100 h.

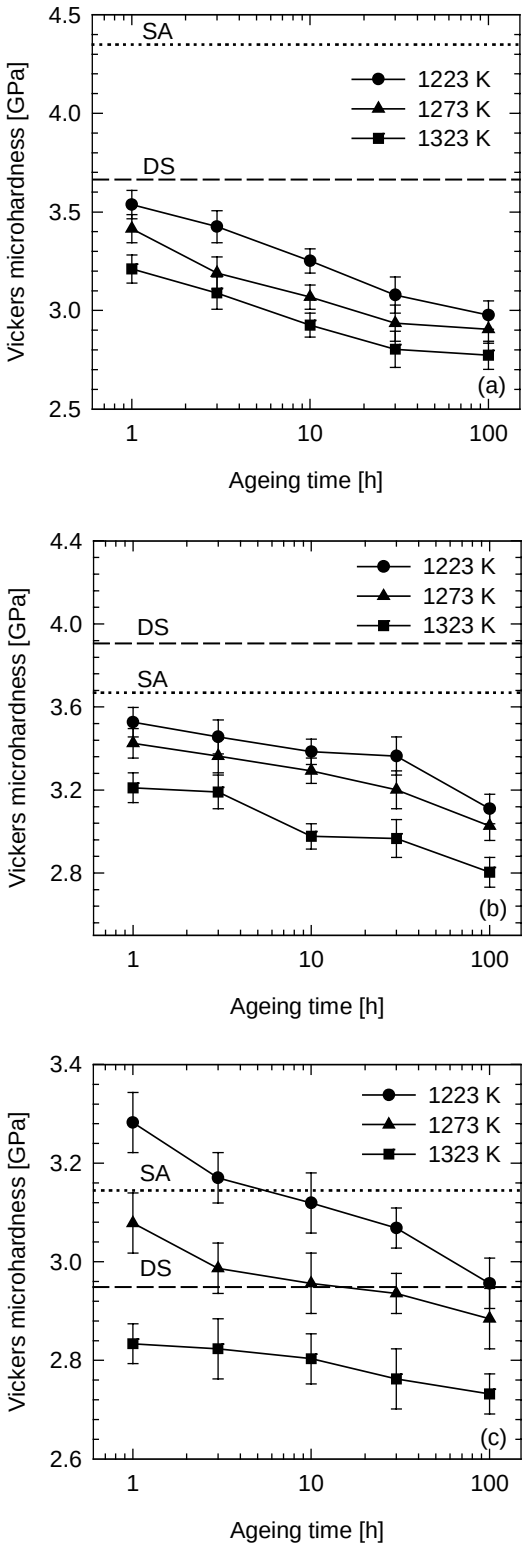

Fig. 9. Dependence of Vickers microhardness on the ageing time: (a) dendrites; (b) interdendritic region – area I; (c) interdendritic region – area II. The dashed and dotted lines in the figures represent microhardness values after directional solidification (DS) and solution annealing (SA), respectively. The ageing temperatures are indicated in the figures.

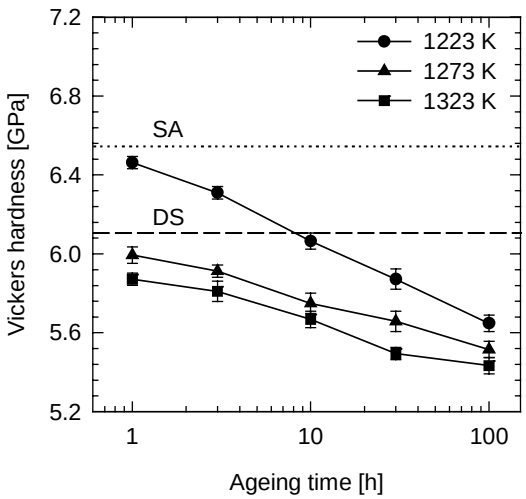

Fig. 10. Dependence of Vickers hardness on the ageing time. The dashed and dotted lines in the figure represent hardness values after directional solidification (DS) and solution annealing (SA), respectively. The ageing temperatures are indicated in the figure.

Figure 9b shows dependence of the microhardness of interdendritic region I on the ageing time. The microhardness decreases with increasing ageing time and temperature. All microhardness values measured in this region for the aged specimens are lower that those of DS (dashed line) or SA (dotted line) ones. The decrease of the microhardness when compared to that of DS specimens can be mainly attributed to the change of morphology γ/γ' microstructure from the cuboidal γ' precipitates in the γ matrix (typical for heat-treated nickel based superalloys) to the γ' matrix with elongated γ particles. In the interdendritic region I, a minimum microhardness value of 2.8 GPa is achieved after ageing at 1323 K for 100 h.

Figure 9c shows evolution of microhardness with the ageing time in the interdendritic region II. The microhardness decreases with increasing ageing time and temperature. A minimum microhardness of 2.73 GPa is achieved after ageing at 1323 K for 100 h. It is clear from Fig. 9c that the ageing at 1223 K up to 100 h and at 1273 K up to 30 h increases the microhardness when compared to that of DS samples (dashed line). The microhardness increase can be attributed to the precipitation strengthening of the γ' matrix by lath-shaped α-Cr particles. Lower microhardness values after ageing at 1323 K when compared to those of DS and SA specimens can be explained by overageing effect.

Figure 10 shows dependence of Vickers hardness on the ageing time. The hardness decreases with increasing ageing time and temperature. While all hardness values measured after ageing at 1273 and 1323 K are lower than that of DS specimens (dashed line), age-

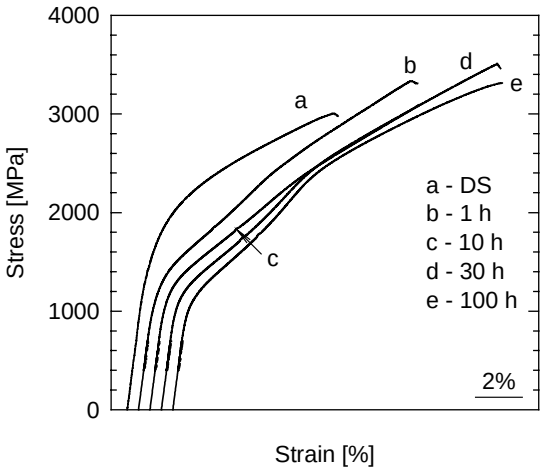

Fig. 11. Examples of engineering compressive stress-strain curves for specimens after directional solidification (DS) and ageing at 1323 K. The ageing time is indicated in the figure.

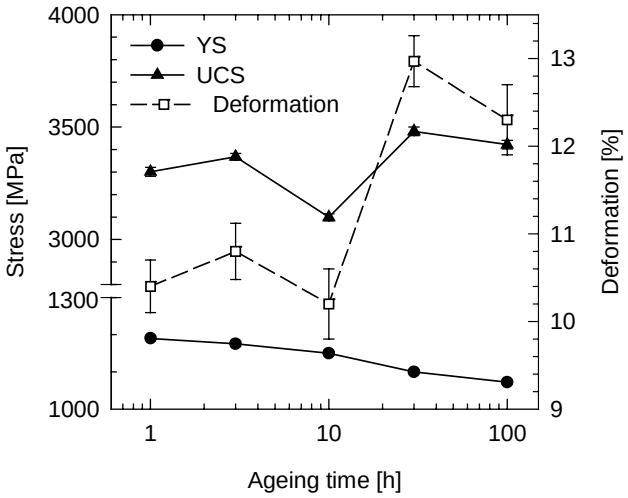

Fig. 12. Variation of offset compressive yield strength (YS), ultimate compressive strength (UCS) and compressive plastic deformation to fracture with the ageing time for specimens aged at 1323 K.

ing for 10 h or longer time at 1223 K is required to soften the alloy. A minimum hardness of 5.43 GPa is achieved after ageing at 1323 K for 100 h.

3.2.2. Effect of heat treatments on room-temperature compressive properties

Figure 11 shows examples of room-temperature compressive engineering stress-strain curves for specimens after directional solidification and ageing at 1323 K. It is clear that the shape of compressive curves is significantly affected by the applied heat treatments. Figure 12 shows dependence of 0.2% offset compressive yield strength (YS), ultimate compressive strength (UCS) and plastic deformation to fracture on the ageing time for the specimens aged at 1323 K. It should be noted that the data presented in this figure represent average values from five specimens tested at each regime. The average YS continuously decreases with the increasing ageing time. On the other hand, the evolution of average UCS and deformation to fracture with the ageing time is not monotonous. Minimum values are achieved after ageing for 10 h and maximum after ageing for 30 h. Ageing at 1323 K decreases the yield strength but increases deformation to fracture and ultimate compressive strength when compared to those of 1300 MPa, 3004 MPa and 7.6%, respectively, reported for DS specimens before heat treatments [24].

Figure 13 shows the typical true stress-true strain compressive curves for DS and HT specimens. For HT specimen, three regions designated as I, II, and III can be clearly distinguished on the compressive curve. Only two regions designated as II and III characterize the deformation curve of DS specimen. In the region I, strain hardening characteristics of HT specimens

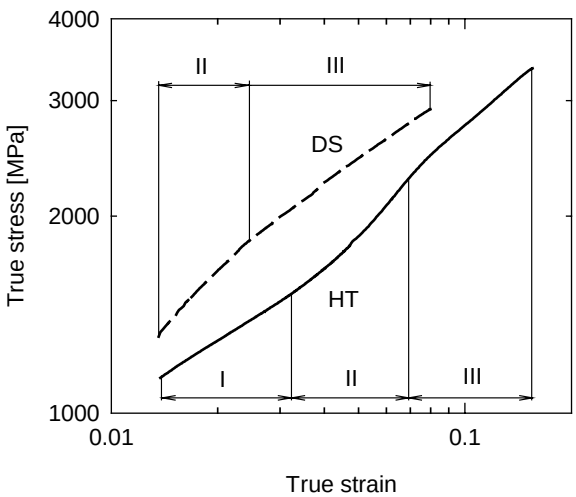

Fig. 13. Examples of compressive true stress-true strain curves for directionally solidified (DS) and heat-treated (HT) specimens.

can be evaluated from average work hardening rate $\Theta = \Delta\sigma_t - \Delta\varepsilon_t$ and average strain hardening exponent n defined by the well-known Hollomon relation [31]

$$\sigma_t = K_1 \varepsilon_t^n, \tag{1}$$

where σ_t is the true stress, ε_t is the true strain and K_1 is the strength factor. Analysis of the deformation curves of HT specimens revealed that the strain hardening exponent n varies between 0.34–0.36 and average work hardening rate Θ between 1870 and 2020 MPa. The measured values of n and Θ are comparable

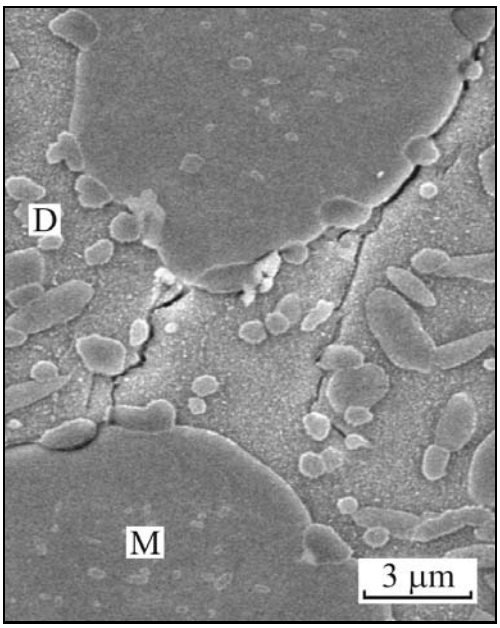

Fig. 14. SEM micrographs showing cracks formed at dendritic-interdendritic interfaces and within the β dendrite in compressive specimen aged at 1323 K for 100 h during testing to a strain of 10 %. D – dendrite, M – interdendritic region.

with those of 0.31–0.38 and 1950–2260 MPa, respectively, reported for tensile specimens of DS and HT Ni-20.2Al-8.2Cr-2.4Fe (in at.%) alloy [32]. In the region II, faster increase of the true stress with increasing true strain can be attributed to a development of local plastic instabilities in both DS and HT specimens. In the region III, moderate increase of the true stress with increasing true strain is caused by initiation and growth of cracks within more brittle β dendrites. Figure 14 shows cracks formed along the dendritic-interdendritic interfaces and within the β matrix during straining in the region III.

3.2.3. Relationship between Vickers hardness and compressive yield strength

Figures 10 and 12 show that both Vickers hardness and compressive yield strength decrease with increasing ageing time at 1323 K. Hence, the yield strength can be correlated with the hardness values when a certain amount of work hardening below the indentor is achieved. Figure 15 shows dependence of yield strength on Vickers hardness for the DS and HT specimens. The yield strength YS increases linearly with increasing hardness HV according to a relationship

$$YS = K_2 + K_3 HV, \tag{2}$$

where K_2 and K_3 are material constants. Linear regression analysis leads an equation for the yield

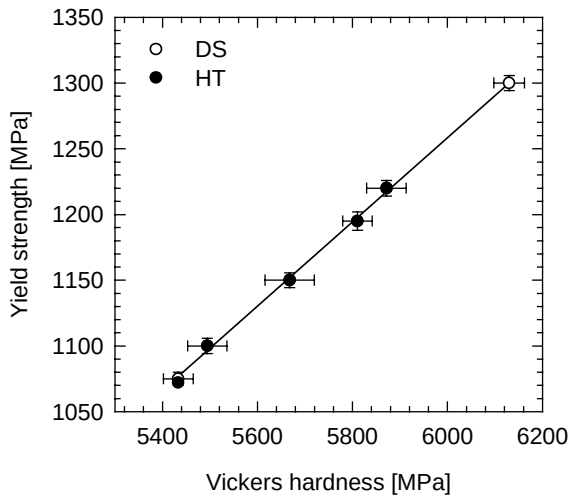

Fig. 15. Dependence of offset compressive yield strength on the Vickers hardness for directionally solidified (DS) and heat-treated (HT) specimens. D – dendrite, M – interdendritic region.

strength in the form

$$YS = -679 + 0.32HV. \tag{3}$$

Correlation coefficient r^2 of this fit is 0.98. Equation (3) allows mechanical properties of the DS and HT ingots to be predicted from simple Vickers hardness measurements.

4. Discussion

4.1. Microstructure evolution during heat treatments

After solution annealing at 1483 K for 2 h and quenching, the size and distribution of spherical α-Cr and needle-like γ' precipitates within the dendrites can be very well controlled by ageing at lower temperatures. During early stages of ageing at temperatures ranging from 1223 to 1323 K, martensitic β'-phase transforms to the β-phase. The ageing leads to coarsening of α-Cr and γ' precipitates within the dendrites and to precipitation of α- and γ'-phases within the interdendritic region. As shown recently by Lapin and Vaňo [28] for DS Ni-22.2Al-8.1Cr-5Ti-0.8Mo-0.6Zr (in at.%) alloy, the growth of α-Cr precipitates within the β dendrites follows $d^3 \propto t$ kinetics with the activation energy for coarsening of 310 kJ/mol, where d is the particle diameter and t is the ageing time. The growth of γ' precipitates follows $d^4 \propto t$ kinetics with the activation energy for coarsening of 250 kJ/mol.

On the other hand, the maximum solution annealing temperature of 1483 K is too low and annealing time of 2 h is too short to homogenize completely

the interdendritic region. As applied for many DS Ni-based superalloys [10–12], several significantly longer solution annealing steps might be required for the studied alloy to avoid incipient melting and achieve homogenous γ/γ'-α type of microstructure in the interdendritic region after heat treatments.

4.2. Mechanical properties

Previous investigations on multiphase intermetallic alloys showed that γ'-phase significantly improves ductility of inherently brittle β- and β'-phases. In DS β-γ' and γ/γ'-β alloys, Misra et al. [33–35] showed that a part of ductility results from intrinsic mechanisms such as slip transfer from the γ'- to β-phase. Remaining part of ductility is governed by extrinsic toughening mechanisms such as crack blunting and crack bridging. In the case of the present alloy, the compressive axis of specimens was close to the $\langle 001 \rangle$ and $\langle 110 \rangle$ crystallographic directions of the β dendrites and γ'/γ matrix, respectively. Young's modulus of the compressive specimen E in a direction parallel to $\langle 001 \rangle$ growth direction of dendrites can be estimated from the rule of mixtures in the form

$$E = V_\beta E_\beta + (1 - V_\beta)\, E_{\gamma'/\gamma}, \tag{4}$$

where V_β is the volume fraction of dendrites. Young's modulus $E_{\gamma'/\gamma}$ of the γ'/γ matrix in the $\langle 110 \rangle$ direction and E_β of the β-phase in the $\langle 001 \rangle$ direction were reported to be 139 and 88 GPa [36, 37], respectively. Taking volume fraction of dendrites for DS specimens of 58.3 vol.% (see Fig. 7), one can calculate the Young's modulus of the compressive specimens to be 109.3 GPa. This calculated value is in a reasonable agreement with that of 107.3 ± 3.3 GPa measured on the compressive specimens (15 independent measurements).

Since the Young's modulus of the γ'/γ matrix is higher than the modulus of the β-phase, during uniform straining of both components the stresses carried by the γ'/γ matrix are higher than those of dendrites. We assume that the dislocations generated in the γ'/γ matrix on the $\{111\}$ slip planes start piling up at the dendritic-interdendritic interfaces. Pile-up stresses in the γ'/γ matrix can preferentially nucleate dislocations on softer $\{110\}\langle 001 \rangle$ instead of harder $\{110\}\langle 111 \rangle$ slip systems of the β-phase [34]. Such slip transfers are also assumed to operate in the present alloy during straining in the regions I and II and result in relatively high plastic deformation to fracture of the compressive specimens. However, detailed TEM analysis has to be performed on compressive specimens to confirm the described deformation mechanisms. Once microcracks nucleate at dendritic-interdendritic interfaces in the region III, α-Cr and γ' precipitates blunt the crack tips, cause crack deviation or stop cracks in the β matrix, as shown in Fig. 14. In addition, some elongated γ' precipitates bridging the crack provide additional plastic strain for the material before its failure. Higher ductility of HT specimens can be explained by coarser γ' and α-Cr precipitates within dendrites and lower volume fraction of inherently brittle β dendrites.

5. Conclusions

The investigation of the effect of heat treatments on the microstructure and mechanical properties of DS multiphase intermetallic Ni-21.9Al-8.1Cr-4.2Ta-0.9Mo-0.3Zr (in at.%) alloy yielded the following conclusions:

1. Two-step solution annealing of DS alloy at 1373 K for 100 h and at 1483 K for 2 h leads to dissolution of spherical α-Cr and needle-like γ' precipitates in the β dendrites. In the interdendritic region, dissolution of Cr-based particles and formation of irregular shaped γ areas in the vicinity of dendritic-interdendritic interfaces are observed. However, the solution annealing temperature of 1483 K is too low and annealing time of 2 h is too short to homogenize completely multiphase $\gamma'/\gamma + \alpha$ interdendritic region.

2. During ageing at temperatures from 1223 to 1323 K the growth of spherical of α-Cr and needle-like γ' precipitates in the β dendrites was observed. In the interdendritic region, the ageing leads to intensive precipitation of lath-shaped α-Cr, formation of irregular shaped Cr-based particles and transformation of γ matrix with γ' precipitates to the γ' matrix with needle-like γ precipitates in the interdendritic region.

3. The heat treatments consisting of two-step solution annealing and ageing can be successfully applied to soften the DS alloy. After solution annealing, all Vickers microhardness values of dendrites after ageing in the temperature range from 1223 to 1323 K and hardness values after ageing at 1273 and 1323 K are lower than those measured after directional solidification.

4. A linear relationship between the Vickers hardness and compressive yield strength was determined for DS and HT specimens, which allows the mechanical properties of the alloy to be predicted from simple hardness measurements.

5. The shape of compressive deformation curves is significantly influenced by heat treatments. Compressive yield strength decreases with increasing ageing time at 1323 K. The maximum ultimate compressive strength and deformation to fracture are achieved after ageing at 1323 K for 30 h. This heat treatment increases ultimate compressive strength by 16 %, plastic deformation to fracture by 71 % but decreases yield strength by 18 % when compared to those of DS specimens.

Acknowledgements

The authors gratefully acknowledge the financial support of the Slovak Grant Agency for Science under the contract VEGA 2/4166/24 and Ministry of Education, Youth and Sports of the Czech Republic under the contract MSM6198910013.

References

[1] SIKKA, V. K.—SANTELLA, M. L.—ANGELINI, P.—MENGEL, J.—PETRUSHA, R.—MARTOCCI, A. P.—PANKIW, R. I.: Intermetallics, *12*, 2004, p. 837.
[2] SIKKA, V. K.—DEEVI, S. C.—VISWANATHAN, S.—SWINDEMAN, R. W.—SANTELLA, M. L.: Intermetallics, *8*, 2000, p. 1329.
[3] STOLOFF, N. S.—LIU, C. T.—DEEVI, S. C.: Intermetallics, *8*, 2000, p. 1313.
[4] PRAHL, J.—HAUŠILD, P.—KARLÍK, M.—CRENN, J. F.: Kovove Mater., *43*, 2005, p. 134.
[5] KRATOCHVÍL, P.—HANUS, P.—HAKL, J.—VLASÁK, T.: Kovove Mater., *42*, 2004, p. 73.
[6] HAUŠILD, P.—KARLÍK, M.—NEDBAL, I.—PRAHL, J.: Kovove Mater., *42*, 2004, p. 156.
[7] LAPIN, J.: Kovove Mater., *43*, 2005, p. 81.
[8] LAPIN, J.—PELACHOVÁ, T.: Kovove Mater., *42*, 2004, p. 143.
[9] HARDING, R. A.: Kovove Mater., *42*, 2004, p. 225.
[10] LUKÁŠ, P.—ČADEK, J.—KUNZ, L.—SVOBODA, M.—KLUSÁK, J.: Kovove Mater., *43*, 2005, p. 5.
[11] MALDINI, M.—LUPINC, V.—ANGELLA, G.: Kovove Mater., *42*, 2004, p. 283.
[12] MALDINI, M.—LUPINC, V.—ANGELLA, G.: Kovove Mater., *42*, 2004, p. 21.
[13] CAHN, R. W.: Phil. Trans. R. Soc. Lond., *A351*, 1995, p. 497.
[14] LAPIN, J.: Kovove Mater., *40*, 2002, p. 209.
[15] VAŇO, A.—PELACHOVÁ, T.: Kovove Mater., *42*, 2004, p. 121.
[16] LAPIN, J.: Scripta Mater., *51*, 2004, p. 733.
[17] LAPIN, J.—BAJANA, O.: Kovove Mater., *43*, 2005, p. 169.
[18] FLORIAN, M.: Kovove Mater., *41*, 2003, p. 73.
[19] IŽDINSKÝ, K.—IVAN, J.—ZEMÁNKOVÁ, M.—CSUBA, A.—MINÁR, P.—IŽDINSKÁ, Z.: Kovove Mater., *42*, 2004, p. 316.
[20] PALM, M.—PREUHS, J.—SAUTHOFF, G.: J. Mater. Proc. Technol., *136*, 2003, p. 105.
[21] PALM, M.—PREUHS, J.—SAUTHOFF, G.: J. Mater. Proc. Technol., *136*, 2003, p. 114.
[22] LAPIN, J.—PELACHOVÁ, T.—BAJANA, O.: Intermetallics, *8*, 2000, p. 1417.
[23] LAPIN, J.: J. Mater. Proc. Technol., *117*, 2001 – Special issue CD-ROM.
[24] LAPIN, J.—MAREČEK, J.: Intermetallics, *14*, 2006 (in press).
[25] LAPIN, J.—ONDRÚŠ, Ľ.—NAZMY, M.: Intermetallics, *10*, 2002, p. 1019.
[26] LAPIN, J.—MAREČEK, J.: in preparation.
[27] LAPIN, J.: Intermetallics, *14*, 2006 (in press).
[28] LAPIN, J.—VAŇO, A.: Scripta Mater., *50*, 2004, p. 571.
[29] LAPIN, J.—WIERZBINSKI, S.—PELACHOVÁ, T.: Intermetallics, *7*, 1999, p. 705.
[30] IŽDINSKÝ, K.—DUFEK, J.—IVAN, J.—ZEMÁNKOVÁ, M.—MINÁR, P.—IŽDINSKÁ, Z.: Kovove Mater., *41*, 2003, p. 365.
[31] HOLLOMON, J. H.: Trans. AIME, *162*, 1945, p. 268.
[32] LAPIN, J.: Intermetallics, *5*, 1997, p. 615.
[33] MISRA, A.—GIBALA, R.: Metall. Mater. Trans. A, *28A*, 1997, p. 795.
[34] MISRA, A.—GIBALA, R.—NOEBE, R. D.: Metall. Mater. Trans. A, *30A*, 1999, p. 1003.
[35] MISRA, A.—GIBALA, R.: Metall. Mater. Trans. A, *30A*, 1999, p. 991.
[36] DICKSON, R. W.—WACHTMAN, J. B.—COPLEY, S. M.: J. Appl. Phys., *40*, 1969, p. 2276.
[37] STOLOFF, N. S.—SIKKA, V. K.: Physical Metallurgy and Processing of Intermetallic Compounds. New York, Chapman and Hall 1996, p. 169.